

3D Point Cloud Registration with Learning-based Matching Algorithm

Rintaro Yanagi^{1,2} Atsushi Hashimoto² Shusaku Sone² Naoya Chiba^{2,3} Jiaxin Ma²
Yoshitaka Ushiku²

¹Hokkaido University ²OMRON SINIC X Corp. ³Tohoku University

yanagi@lmd.ist.hokudai.ac.jp, atsushi.hashimoto@sinicx.com, chiba@nchiba.net

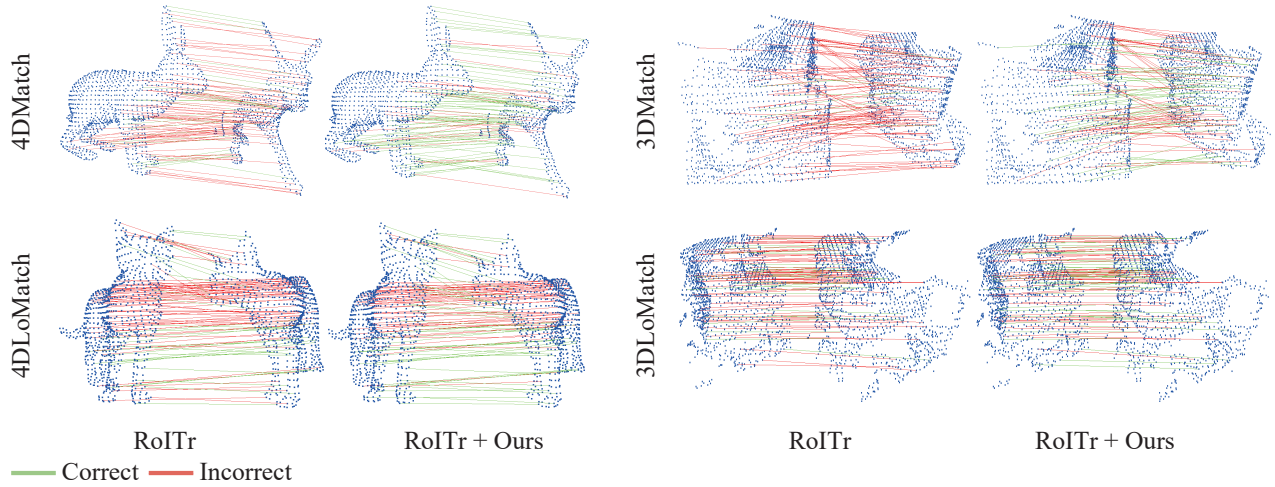


Figure 1. Visualization of improvement by our learning-based matching algorithm on diverse datasets. We randomly select the sample to avoid cherry-picking. Here, green lines show the exact matches, while red are failures.

Abstract

We present a novel differential matching algorithm for 3D point cloud registration. Instead of only optimizing the feature extractor for a matching algorithm, we propose a learning-based matching module optimized to the jointly-trained feature extractor. We focused on edge-wise feature-forwarding architectures, which are memory-consuming but can avoid the over-smoothing effect that GNNs suffer. We improve its memory efficiency to scale it for point cloud registration while investigating the best way of connecting it to the feature extractor. Experimental results show our matching module’s significant impact on performance improvement in rigid/non-rigid and whole/partial point cloud registration datasets with multiple contemporary feature extractors. For example, our module boosted the current SOTA method, RoITr, by +5.4%, and +7.2% in the NFMR metric and +6.1% and +8.5% in the IR metric on the 4DMatch and 4DLoMatch datasets, respectively. Code is publicly available¹.

¹<https://github.com/omron-sinicx/weavenet>

1. Introduction

3D point cloud registration lies at the core of many downstream 3D computer vision applications such as motion transfer [32], shape editing [20], and object localization for industrial robots [5]. The challenge of 3D point cloud registration comes from the sparseness, sensing difficulty, and non-rigid deformation of the 3D point cloud data [2, 29, 50]. Recent registration methods have tackled the challenges using deep-learning-based models, and their performance has been improved.

The primary 3D point cloud registration method consists of a feature extractor and a matching algorithm. The former module extracts point-wise features, which organize a similarity matrix fed to the latter module of the matching algorithm. The algorithm’s output is a correspondence matrix indicating point-wise correspondence between two point clouds. The principal idea of the algorithm is to solve the linear assignment problem, and the Hungarian algo-

rithm [15] is known as an optimal solver for the problem. However, the algorithm must be differentiable for back-warding a loss at the matching results to the feature extractor. Hence, the Sinkhorn algorithm [3], a differentiable approximation of the Hungarian algorithm, was first applied to this task. Then, it was reported that some heuristic operations, such as DeSmooth [47] and dual-softmax [26] works better than the Sinkhorn algorithm. They are used in recent SOTA methods [19, 44].

This paper proposes a learning-based matching algorithm instead of the recent hand-crafted heuristics. The Sinkhorn algorithm, like the Hungarian algorithm, optimally solves the matching problem independently of the feature extractor during inference. However, it is defeated by the heuristics of DeSmooth and dual-softmax. This observation suggests that such independent optimization is sub-optimal. On the other hand, the heuristics algorithms are fixed regardless of the feature extractor. Thus, they are not actively optimized for the trained feature extractor. How does it work if we have an algorithm that can be optimized flexibly depending on the feature extractor? We aim to answer this question by providing such an architecture with experimental results.

The contribution of this paper is threefold.

1. We propose to combine a learning-based matching algorithm with a feature extractor for the first time.
2. We improve the memory efficiency of an existing bipartite-matching neural network to scale it for 3D point cloud registration.
3. We boosted the performance for versatile methods and achieved a SoTA performance.

2. Related work

2.1. Feature extraction from 3D Point Cloud

There are many tasks on 3D point clouds, such as shape classification, 3D object detection, and point cloud segmentation, in addition to registration [10, 11]. Early stage studies for 3D point cloud data have focused on the design of hand-crafted point-wise features (a.k.a., local descriptors) [14, 33, 40, 41] and key point detection [51]. A comprehensive survey [9] has revealed their characteristics; however, it also reports their limitation on performance caused by noise, clutter, fluctuation in resolutions, and occlusions.

The recent growth in deep learning methods has led to significant improvements in feature extraction [10, 11], which has also impacted on the registration task. First-generation deep-learning-based feature extractors for 3D matching relied on the architecture developed for 2D images, where point cloud data are projected onto an image plane as the RGB-D image format [6] or handled 3D shape by voxel-based 3D CNNs [22, 46]. Then, PointNet [24] and

DeepSets [45] were proposed, which enabled us to extract point-wise features directly from unstructured point clouds. Then second-generation studies enhanced the techniques for various tasks on 3D point clouds [12, 21, 25, 35, 37–39, 48].

Registration-specific techniques for feature extractors have been also developed. Huang *et al.* [13] introduced a cross-attention mechanism, which enables to extract features interactively between two point clouds. The idea is succeeded to following studies [18, 19, 43]. Another registration-specific factor is the way of registration after extracting features. There are roughly two types of registration approaches: parametric registration (i.e., rigid transform) [1, 28, 36] and non-parametric registration [42, 47, 49]. The parametric approach formulates the problem as estimating parameters that represent the deviation of two point clouds. The non-parametric approach represents such deviation by individual correspondence of each point in two point clouds. This paper focuses on the non-parametric approach because it can deal with non-rigid cases, and the result can be a good initialization of the parametric approach even for rigid cases. The non-parametric approach requires a differentiable matching algorithm to optimize the feature extractor to the matching algorithm. We propose a method to optimize a matching algorithm to the feature extractor as the feature extractor is optimized to the matching algorithm.

2.2. Differentiable matching algorithm

The combination of feature extractor and differentiable matching algorithm is applied not only for 3D point clouds but also for other registration tasks in computer vision. SuperGlue [27] is a representative 2D RGB image registration method that introduced the **Sinkhorn** algorithm for a registration task with deep-learning-based feature extractors. In the next year’s CVPR, two papers experimentally reported that heuristic matching operations outperform the Sinkhorn algorithm. The first report is by Zeng *et al.* [47]. They proposed the **DeSmooth** operation, which works better than the Sinkhorn algorithm on the 3D point cloud registration task. The second one is by Sun *et al.* [31]. They found that the **dual softmax** operation [26] works better on the 2D image registration task. Dual softmax is introduced to 3D point cloud registration by **Lepard** [18]. Its subsequent study, **LNDP** [19], also uses dual softmax. The current SOTA method, RoITr [44], has coarse and fine matching modules inside, following CoFiNet [43]. In the original CoFiNet, Sinkhorn was used for coarse matching, which RoITr replaced with dual softmax. Inspired by the fact that a heuristic operation of dual softmax outperforms Sinkhorn, this study investigates the possibility of a learning-based matching algorithm.

Despite the popularity of the registration task in the vision community, learning-based matching algorithms have

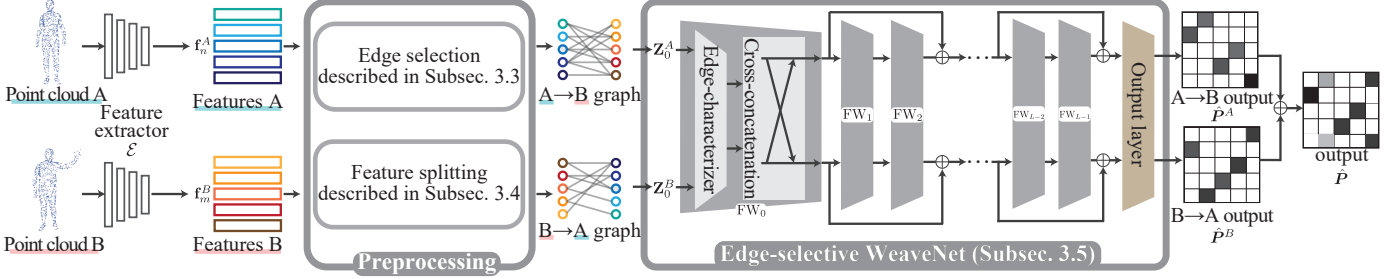


Figure 2. Entire flow of the proposed method. Extracted features are selected to improve memory efficiency Sec. 3.3 and split into components for distance calculation and uncertainty representation Sec. 3.4. Then, pre-processed features are fed to a memory-efficient WeaveNet module, which can process sparse bipartite graphs obtained at edge selection.

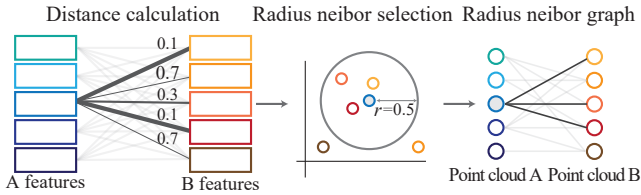


Figure 3. Radius-neighbor-based edge selection.

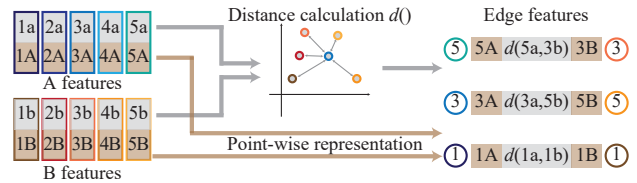


Figure 4. Feature splitting to compress initial edge-wise feature.

not yet been explored. The reason is the difficulty in treating bipartite graphs with graph neural networks (GNNs). It is known that general GNNs suffer from the over-smoothing problem, specifically when the graph is dense [17, 23]. Unfortunately, a bipartite graph is always dense, and GNNs are not effective for this problem.

Among such situations, we found two possible architectures for our purpose: Deep Bipartite Matching (DBM) [7] and WeaveNet [30], both proposed to approximately solve NP-hard matching problems. They avoid the over-smoothing problem by preserving edge-wise features. Since the smoothing effect occurs at aggregating each vertex's feature with its neighbors, forwarding features between neighbors (edge-wise features) without aggregation resolves the problem. However, this strategy has an apparent shortcoming of memory consumption and is not applicable to a large-size matching problem such as 3D point cloud registration. This study proposes to connect feature extractors with WeaveNet in a memory-efficient way and scale it for 3D point cloud registration.

3. Learning-based Matching Algorithm

As introduced in the previous subsection, we develop a learning-based matching algorithm based on WeaveNet (WN) [30], which we call Edge-Selective WN (ESWN). After giving the problem formulation in Sec. 3.1, we explain the basic flow of matching calculation through a feature extractor \mathcal{E} and a WN-based matching module \mathcal{M} in Sec. 3.2.

\mathcal{M} is modified in a memory-efficient form of ESWN in Sec. 3.3. Then, Sec. 3.4 further reduces the memory usage at the connection of \mathcal{E} and \mathcal{M} . Finally, we give a detailed architecture design of the ESWN structure in Sec. 3.5.

3.1. Formal Problem Statement

Let \mathbf{X}^A and \mathbf{X}^B be point clouds with sizes N and M , respectively. We refer to the n -th element in \mathbf{X}^A as $\mathbf{x}_n^A \in \mathcal{R}^{D_x}$ ($n = 1, \dots, N$) and the m -th element in \mathbf{X}^B as $\mathbf{x}_m^B \in \mathcal{R}^{D_x}$ ($m = 1, \dots, M$), where $D_x = 3$ when each point is given by its position in 3D space. The task of 3D point cloud registration is to estimate a correspondence matrix $\mathbf{P} = [p_{n,m}]_{N \times M}$ from the inputs \mathbf{X}^A and \mathbf{X}^B .

3.2. Point cloud matching via \mathcal{E} and \mathcal{M}

For each \mathbf{x}_n^A , a WN-based matching module \mathcal{M} works to find a correct partner in \mathbf{X}^B (and similarly, in \mathbf{X}^A for each \mathbf{x}_m^B). First of all, the features \mathbf{f}_n^A (resp. \mathbf{f}_m^B) of each point \mathbf{x}_n^A (resp. \mathbf{x}_m^B) are calculated by a feature extractor \mathcal{E} as follows: $\mathbf{f}_n^A = \mathcal{E}(\mathbf{x}_n^A)$, $\mathbf{f}_m^B = \mathcal{E}(\mathbf{x}_m^B)$.

Let us consider a directional bipartite graph $G(\mathbf{V}^A, \mathbf{V}^B, \mathbf{E}^{A \rightarrow B}, \mathbf{E}^{B \rightarrow A})$ where $\mathbf{V}^A = \{\mathbf{f}_n^A\}$ and $\mathbf{V}^B = \{\mathbf{f}_m^B\}$ are two sides of vertices, $\mathbf{E}^{A \rightarrow B}$ is the set of edges from side A to B, and $\mathbf{E}^{B \rightarrow A}$ is the set of edges from B to A. Then, using $\mathbf{E}^{A \rightarrow B}$ and $\mathbf{E}^{B \rightarrow A}$, we generate $\{\mathbf{z}_{0,n,m}^A | \{n, m\} \in \mathbf{E}^{A \rightarrow B}\}$ by a connecting function g as $\mathbf{z}_{0,n,m}^A = g(\mathbf{f}_n^A, \mathbf{f}_m^B)$ (resp. $\{\mathbf{z}_{0,m,n}^B | \{m, n\} \in \mathbf{E}^{B \rightarrow A}\}$ by $\mathbf{z}_{0,m,n}^B = g(\mathbf{f}_m^B, \mathbf{f}_n^A)$).

The calculated $\mathbf{z}_{0,n,m}^A$ and $\mathbf{z}_{0,m,n}^B$ are fed to \mathcal{M} and \mathcal{M} outputs $\hat{\mathbf{P}}$, an estimation of the correspondence matrix. Since \mathcal{M} preserved edge-wise features at each layer, its computational graph holds $N \times M$ features at each layer, where $N = M = 1024$ in a standard task of point cloud registration task. Clearly, storing 1M+ features at each stacked layer is intractable even with latest GPUs. Our challenge here is to seek the best way to jointly optimize \mathcal{E} and \mathcal{M} with lower memory consumption with M .

3.3. Edge selection for memory efficiency

We expect that edge pruning impacts on improving memory efficiency of M . Keeping edges of correspondence candidates and removing those with no chance seems feasible by checking the similarity matrix obtained between V^A and V^B .

There are several options for this edge selection. Namely, preserving k -nearest neighbors, k -reciprocal neighbors, and r -radius neighbor of each point. In this study, we considered that k -nearest and k -reciprocal neighbors are not enough memory efficient or difficult to adjust k because features from a well-trained \mathcal{E} will not require many candidates, thus a large k , but it is hard to train such \mathcal{E} with a small k . In other words, controlling candidates with k will require severe hyper-parameter tuning.

Instead, we adopted r -radius neighbors, where r is the distance threshold for selection (Fig. 3). We identify the r -radius neighbors based on the $d(\mathbf{f}_n^A, \mathbf{f}_m^B)$, with a distance function d . Even with fixed r , the number of candidates flexibly varies at each stage of training and based on the uncertainty of each sample. Formally, we describe this as $\mathbf{E}^{A \rightarrow B} = \{\{n, m\} | d(\mathbf{f}_n^A, \mathbf{f}_m^B) \leq r\}$, and $\mathbf{E}^{B \rightarrow A} = \mathbf{E}^{A \rightarrow B}$ since $d(\mathbf{f}_n^A, \mathbf{f}_m^B) = d(\mathbf{f}_m^B, \mathbf{f}_n^A)$.

3.4. Feature splitting for memory efficiency

The original WeaveNet paper reports that it can approximate NP-hard problems with lightweight edge-wise features (i.e., < 32 for any l -th layers edge-wise feature $\mathbf{z}_{l,n,m}^A$). However, typical \mathcal{E} for 3D point cloud registration has more than 256 channels, which is excessive for \mathcal{M} .

Hence, we compress the information by the distance $d(\mathbf{f}_n^A, \mathbf{f}_m^B)$. If we only pass the distance information, it is hard for \mathcal{M} to consider uncertainty on $d(\mathbf{f}_n^A, \mathbf{f}_m^B)$. Hence, we split the extracted features \mathbf{f}_n^A into $\mathbf{f}_n^{A_{\text{dis}}}$ and $\mathbf{f}_n^{A_{\text{point}}}$ (similarly, \mathbf{f}_m^B into $\mathbf{f}_m^{B_{\text{dis}}}$ and $\mathbf{f}_m^{B_{\text{point}}}$). As shown in Fig. 4, we further reduce the memory consumption by calculating the distance on a feature split $\mathbf{f}_n^{A_{\text{dis}}}$ while bypassing the uncertainty information with another split $\mathbf{f}_n^{A_{\text{point}}}$, where we refer to \mathcal{D}_s as a hyperparameter of the $\mathbf{f}_n^{A_{\text{point}}}$'s channel size.

Based on the above idea, the connecting function g is defined as

$$g(\mathbf{f}_n^{A_{\text{point}}}, \mathbf{f}_m^{B_{\text{point}}}) = \text{cat}(\mathbf{f}_n^{A_{\text{point}}}, d(\mathbf{f}_n^{A_{\text{dis}}}, \mathbf{f}_m^{B_{\text{dis}}}), \mathbf{f}_m^{B_{\text{point}}}), \quad (1)$$

where $\text{cat}(\cdot)$ is feature concatenation.

3.5. Network architecture

A basic idea of WN is to represent an edge-wise feature as an element in the edge set that shares the same node as the source end-point. This is realized following the architecture proposed in PointNet [24] (or DeepSets [45]) inside each layer and for edge node-sharing edge set.

Let $\text{FW}_l : \{\mathbf{Z}_l^A, \mathbf{Z}_l^B\} \rightarrow \{\mathbf{Z}_{l+1}^A, \mathbf{Z}_{l+1}^B\}$ be the l -th layer of WN, called *feature weaving layer*. We organize \mathcal{M} by stacking L feature weaving layers ($l = 0, \dots, L-1$) and one output layer. Here, the feature weaving layer has two main components: an edge-characterizer and a cross-concatenation.

The edge-characterizer discriminatively extracts features between adjacent nodes with and without aggregation. WN can avoid the over-smoothing problem owing to the forwarding pass without aggregation. We first extract edge features via a trainable linear layer $\phi_l^1(\cdot)$ and max-pooling $\max(\cdot)$ as follows:

$$\mathbf{h}_{l,n}^A = \max_{m_k \in \mathcal{N}(n)} (\phi_l^1(\mathbf{z}_{l,n,m_k}^A)). \quad (2)$$

Here, $\mathbf{h}_{l,n}^A$ is expected to aggregate all the specific characteristics of matching candidates. $\mathbf{h}_{l,n}^A$ is then concatenated to $\mathbf{z}_{l,n,m}^A$ and applied another linear layer $\phi_l^2(\cdot)$ as PointNet or DeepSet. Overall, an edge characterizer is formulated as

$$\mathbf{g}_{l,n,m}^A = \text{act}(\text{BN}(\phi_l^2(\text{cat}(\mathbf{z}_{l,n,m}^A, \mathbf{h}_{l,n}^A)))), \quad (3)$$

where $\text{act}(\cdot)$ and $\text{BN}(\cdot)$ represent pReLU activation and batch normalization, respectively.

The cross-concatenation expands the receptive field by concatenating the features repeatedly across sides A and B at every end of feature weaving layers. Owing to our choice of r -radius neighbor edge selection, $\mathbf{E}^{A \rightarrow B} = \mathbf{E}^{B \rightarrow A}$ and we always have both $\mathbf{g}_{l,n,m}^A$ and $\mathbf{g}_{l,m,n}^B$. Thus, we can define the cross-concatenation in the same manner as the original WN, which is

$$\mathbf{z}_{l+1,n,m}^A = \text{cat}(\mathbf{g}_{l,n,m}^A, \mathbf{g}_{l,n,m}^B), \quad (4)$$

$$\mathbf{g}_{l,n,m}^B = \frac{1}{K} \sum_{m_k \in \mathcal{N}(n)} \mathbf{g}_{l,m_k,n}^B. \quad (5)$$

The output layer finalizes \mathbf{Z}_L^A , the output of the $(L-1)$ stacked feature weaving layers, to be an estimate of the correspondence matrix $\hat{\mathbf{P}}$. This layer first applies the same calculation as in Eq. (2) but without activation. Next, we calculate $\hat{p}_{n,m}^A$ for each $\{n, m\}$ in $\mathbf{E}^{A \rightarrow B}$ as follows:

$$\hat{p}_{n,m}^A = \begin{cases} \mathbf{g}_{L,n,m}^A & \text{if } \{n, m\} \in \mathbf{E}^{A \rightarrow B} \\ 0 & \text{otherwise.} \end{cases} \quad (6)$$

Finally, $\hat{\mathbf{P}}$ is obtained as an average of $\hat{\mathbf{P}}^A$ and $\hat{\mathbf{P}}^B$.

Dataset	Shape	partial?	non-rigid?
4DMatch [18]	Animal		✓
4DLoMatch [18]	Animal	✓	✓
3DMatch [46]	Indoor		
3DLoMatch [13]	Indoor	✓	
Surreal [8]	Human		
Surr.(train)/SHREC [4](test)	Human		✓

Table 1. Diversity of datasets in our experiments.

4. Experiments

We confirmed the effectiveness of our module by testing it with four SOTA methods, including the heuristic matching algorithm on six datasets summarized in Tab. 1. For **4DMatch**, **4DLoMatch**, **3DMatch**, and **3DLoMatch** datasets, we tested our module with three SOTA methods of **Lepard** [18], **LNDP** [19], and **RoITr** [44]. They are originally implemented with **dual softmax (DS)** or the Sinkhorn algorithm, as **the optimal transport function (OT)**. We replace it with **our modified WeaveNet module (WN)**. As yet another evaluation, we combined WN with **CorrNet3D** [47] and evaluated the effect on the **Surreal** and **SHREC** datasets with supervised and unsupervised settings. Through all experiments, we train and test methods following their original experimental settings other than the replaced WN part.

4.1. Rigid/Non-rigid and Whole/Partial conditions

Dataset. We conducted experiments in the matching task of animals (non-rigid) and indoor (rigid) point clouds, following the experiments in [18, 19, 44]. First, experiments on animal point clouds are conducted using the 4DMatch and 4DLoMatch datasets [18]. In this experiment, 1,761 animation sequences are split into 1,232/176/353 as train/valid/test sets, and the test sets are finally split into 4DMatch and 4DLoMatch datasets based on the overlap ratio greater than and less than 45%, respectively.

Second, experiments on the indoor point clouds are conducted using the 3DMatch and 3DLoMatch datasets [13, 46]. 3DMatch contains scan pairs with overlap ratios greater than 30%, while 3DLoMatch contains scan pairs with ratios between 10% and 30%. The 62 indoor scenes are divided into 46/8/8 as train/valid/test sets.

Evaluation metrics. We used the inlier ratio (IR) and non-rigid feature matching recall (NFMR) as the evaluation metrics for 4DMatch and 4DLoMatch dataset following [18, 19, 44]. For the ground-truth matches ($\mathbf{u} \in \mathcal{R}^3, \mathbf{v} \in \mathcal{R}^3$) $\in \mathcal{K}_{gt}$ and the predicted correspondences ($\mathbf{p} \in \mathcal{R}^3, \mathbf{q} \in$

\mathcal{R}^3) $\in \mathcal{K}_{pred}$, IR and NFMR are defined as follows:

$$\text{IR} = \frac{1}{|\mathcal{K}_{pred}|} \sum_{(\mathbf{p}, \mathbf{q}) \in \mathcal{K}_{pred}} [\|W_{gt}(\mathbf{p}) - \mathbf{q}\|_2 < \sigma], \quad (7)$$

$$\text{NFMR} = \frac{1}{|\mathcal{K}_{gt}|} \sum_{(\mathbf{u}, \mathbf{v}) \in \mathcal{K}_{gt}} [\|\Gamma(\mathbf{u}, \mathbf{A}, \mathcal{F}) - \mathbf{v}\|_2 < \sigma], \quad (8)$$

$$\Gamma(\mathbf{u}, \mathbf{A}, \mathcal{F}) = \sum_{A_i \in \text{knn}(\mathbf{u}, \mathbf{A})} \frac{F_i \|\mathbf{p} - \mathbf{A}_i\|_2^{-1}}{\sum_{A_i \in \text{knn}(\mathbf{u}, \mathbf{A})} \|\mathbf{u} - \mathbf{A}_i\|_2^{-1}}, \quad (9)$$

$$\mathcal{F} = \{ \mathbf{q} - \mathbf{p} | (\mathbf{p}, \mathbf{q}) \in \mathcal{K}_{pred} \}, \quad (10)$$

$$\mathbf{A} = \{ \mathbf{p} | (\mathbf{p}, \mathbf{q}) \in \mathcal{K}_{pred} \}, \quad (11)$$

where γ is set as 0.04m, and $\|\cdot\|_2$ and $[\cdot]$ respectively represent the L2-norm and the Iverson bracket.

The IR, feature matching recall (FMR), and rigid registration recall (RR) are used as the evaluation metrics for the 3DMatch and 3DLoMatch datasets following [18]. The FMR indicates the fraction of pairs with $>5\%$ inlier matches with <10 cm residual under the ground truth transformation, and the RR indicates the fraction of scan pairs for which the correct transformation parameters are found with RANSAC.

Implementation details. We replaced the matching algorithms in the conventional methods (dual-softmax (DS) for Lepard and LNDP, and sinkhorn (OT) for RoITr) with our modified WeaveNet module (WN). Our module was optimized with the feature extractors according to the loss function in each method. The parameters in the equations are set as $r = 0.5$, $\mathcal{D}_s = 16$, and $L = 10$. Also, we trained the model with the SGD optimizer, a learning rate of 0.015, a batch size of 8, and 15 epochs, which imitates [18, 19, 44]. These are implemented with the PyTorch framework on four Tesla V100 GPUs.

Results on 4DMatch and 4DLoMatch datasets. The experimental results on 4DMatch and 4DLoMatch dataset are shown in Tab. 2 (left side). In the table, we used suffixes of DS, OT, and WN to the baseline model name to show its matching module (e.g., **Lepard-DS** is Lepard’s original implementation while **Lepard-WN** uses our matching module). The table shows that the methods with the WN module constantly outperform their original implementation in both 4DMatch and 4DLoMatch datasets. These results confirmed that replacing the heuristic matching operations with our learning-based matching module significantly improves the performance on the non-rigid point cloud matching tasks.

The average improvements on these three methods are +4.1% and +4.3% in NFMR and IR on 4DMatch, while +6.5% and +6.8% on 4DLoMatch. These results indicate

Method	4DMatch		4DLoMatch		3DMatch			3DLoMatch		
	NFMR(\uparrow)	IR(\uparrow)	NFMR(\uparrow)	IR(\uparrow)	FMR(\uparrow)	IR(\uparrow)	RR(\uparrow)	FMR(\uparrow)	IR(\uparrow)	RR(\uparrow)
Lepard-DS	83.7	82.7	66.9	55.7	98.3	55.5	93.5	84.5	26.0	69.0
Lepard-WN (ours)	86.7	86.1	72.4	62.5	98.4	64.5	95.7	89.6	30.4	74.9
LNDP-DS	85.4	84.5	67.6	57.6	98.1	56.5	92.4	83.1	27.4	71.1
LNDP-WN (ours)	88.7	87.9	73.4	62.8	98.6	65.6	94.1	91.3	33.3	76.2
RoITr-OT	81.3	81.2	67.2	64.8	98.5	80.3	91.0	89.6	54.3	74.2
RoITr-WN (ours)	87.2	87.3	75.3	73.3	98.9	86.8	96.2	90.0	64.4	82.4
Avg. Improvement	+4.1	+4.3	+6.5	+6.8	+0.3	+8.2	+3.0	+4.6	+6.8	+6.4

Table 2. Quantitative evaluation for rigid/non-rigid and whole/partial conditions. The WN-based matching module always outperforms non-learning-based matching algorithms regardless of the choice of base method and datasets with significant margins.

Method	ES	FS	train	eval.	NFMR(\uparrow)	IR(\uparrow)
WN			135.2 GiB	64.3 GiB	89.9	83.3
		✓	124.5 GiB	57.6 GiB	88.6	84.1
	✓		12.3 GiB	6.4 GiB	87.4	85.2
	✓	✓	8.1 GiB	4.5 GiB	87.2	87.3
OT	-	-	4.6 GiB	2.1GiB	81.3	81.2

Table 3. Memory consumption test on 4DMatch with RoITr. ES and FS stand for Edge Selection and Feature Splitting, respectively.

the difficulty of feature extraction and the effectiveness of the learning-based matching algorithm against uncertainty caused under the challenging condition of partial matching.

Results on 3DMatch and 3DLoMatch datasets. Tab. 2 (right side) shows the experimental results on the 3DMatch and 3DLoMatch datasets. Again, methods with the learning-based matching module constantly outperform the baseline models in both 3DMatch and 3DLoMatch datasets with a large margin. These results indicate the versatility of the proposed approach.

The average improvements in these rigid conditions are +0.3%, +8.2%, +3.0% in FMR, IR, and RR on 3DMatch, while +4.6%, +6.8%, +6.4% on 3DLoMatch. Notably, the learning-based matching module has never underperformed the original implementations through all experiments. In addition, FMR on 3DMatch was already more than 98.1% without our module, but it has improved the score by 0.3% on average, which is also outstanding.

4.2. Analysis on Memory Consumption

Our method aimed to improve memory efficiency to scale the original WeaveNet [30] for point cloud registration. Tab. 3 shows an analysis of memory consumption, measured in actual training and inference on 4DMatch with RoITr. The edge selection significantly decreases the memory consumption from 135.2 GiB to 12.3 GiB (-90.9%) at training and from 64.3GiB to 6.4 GiB (-90.0%) at infer-

ence, while the performance is increased in IR and worse in NFMR, thus comparative in total. Feature splitting at the connection between the feature extractor and the matching module further reduces memory consumption from 12.3 GiB to 8.1 GiB (-34.1%) at training and from 6.4 GiB to 4.5 GiB (-29.7%) at inference, with comparative NFMR and improved IR.

The same tendency was observed with different datasets and baselines, as shown in the supplemental material. Overall, the analysis proved that our modification on WeaveNet is effective in both memory efficiency and accuracy. Simultaneously, it revealed that WN still consumes memories about two times more than DS, which is the limitation of our method.

4.3. Systematic Analysis on Feature Uncertainty

We intended to introduce a learning-based matching algorithm to deal with sub-optimality on the linear assignment optimization on the estimated similarity matrix. In other words, the method is designed to deal with the uncertainty inevitably involved in the extracted features.

Aiming to confirm that our method realizes this intention, we conducted a systematic study using 4DLoMatch and 3DLoMatch, whose results are shown in Figs. 5 and 6. In this experiment, we input the same point clouds to both the source and target sides but add Gaussian noise $\mathcal{N}(0, \sigma)$ on the source side data to simulate the uncertainty on features while removing any other effects. The parameter σ is controlled from 0.0 to 1.0 by 0.2 of step-width.

We observed clear performance drop for larger σ in both figures, as intended. Among them, methods using our matching module (WN) always outperformed their original implementations (DS or OT). These results indicate that our intention of uncertainty-tolerant matching was obtained by our method.

4.4. Hyperparameter Validation

Hyperparameter sensitivity against dataset and combined feature extractors is an important factor of our method’s

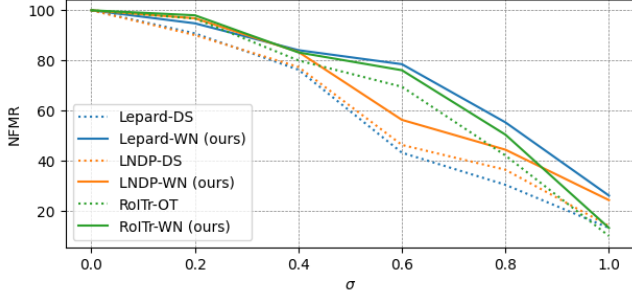


Figure 5. Noise tolerance test on 4DLoMatch. Our WN-based matching algorithm always outperforms its original setting.

Method	4DLoMatch		3DLoMatch			
	NFMR(\uparrow)	IR(\uparrow)	FMR(\uparrow)	IR(\uparrow)	RR(\uparrow)	
OT	67.2	64.8	89.6	54.3	74.2	
WN	$r = 0.1$	69.6	67.1	89.6	60.2	76.0
	$r = 0.5$	75.3	73.3	90.0	64.4	82.4
	$r = 1.0$	70.1	70.3	89.9	61.3	77.7
WN	$L = 6$	68.9	67.9	89.9	58.9	77.8
	$L = 8$	73.4	72.1	90.0	62.1	81.3
	$L = 10$	75.3	73.3	90.0	64.4	82.4
WN	$\mathcal{D}_s = 4$	69.1	70.5	89.5	55.4	79.5
	$\mathcal{D}_s = 16$	75.3	73.3	90.0	64.4	82.4
	$\mathcal{D}_s = 64$	70.4	69.5	89.9	60.3	81.3

Table 4. Study on the impact of hyperparameters with RoITr. We set uncontrolled hyperparameters to our defaults (e.g., when r is varied, we used $L = 10$ and $\mathcal{D}_s = 16$).

utility. We extensively conducted ablation studies on hyperparameter validation. Our method has three hyperparameters, r , L , and \mathcal{D}_s . We used the values directed in Subsec. 4.1 as the defaults. Tab. 4 shows the results with RoITr on 4DLoMatch and 3DLoMatch. In this setting, the default values always outperformed the others regardless of the dataset. We observed the same tendency for the other methods and used these values throughout the experiments in this paper. See supplemental materials for results with other conditions.

We discuss the results in detail. First, r is a parameter controlling edge selection ratio. Small r prunes edges overly, and large r loses the performance gain by edge selection. This property is observed as the lower performance on $r = 0.1$ and 1.0 than $r = 0.5$. Second, L is the number of layers. Generally, the deeper a network is, the more accurate the estimation is. From the result, we confirmed that this expectation is the case with our method. Third, \mathcal{D}_s controls the split ratio of feature vector into components of similarity matrix and uncertainty representation. Too small \mathcal{D}_s disables to represent uncertainty, while too large \mathcal{D}_s

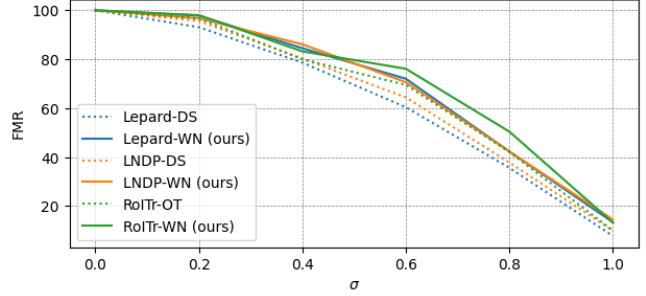


Figure 6. Noise tolerance test on 3DLoMatch. We can see the same tendency with the study on 4DLoMatch in Fig. 5.

leads to a shortage of dimensions for similarity calculation. The result explains this well, as $\mathcal{D}_s = 16$ works better than $\mathcal{D}_s = 4$ and 64 among the 256 channels of the RoITr feature.

4.5. Evaluation with CorrNet3D on Human Shape data

Dataset. We further conducted experiments in both rigid and non-rigid settings with human shape data, following the experiments in [47]. Here, we combined our matching module with CorrNet3D [47], which has supervised and unsupervised training options.

The Surreal dataset [34] is used for rigid human shape setting, which contains 230K point cloud samples for training and 100 samples for testing. The 230K point clouds were randomly paired into 115K training samples, and 100 test pairs were created by randomly rotating and translating the test samples. For the non-rigid settings, the Surreal dataset and the SHREC dataset [16] are used for training and test, which respectively contain 230K and 860 samples. The training samples were the same as in the rigid setting, while the 860 test samples were randomly combined into 430 test pairs. Each point cloud contained 1024 points for all the above datasets.

Evaluation metrics. The corresponding percentage (Corr) under various tolerant errors is used for the evaluation metrics following [47]. The Corr and tolerant errors are defined as follows:

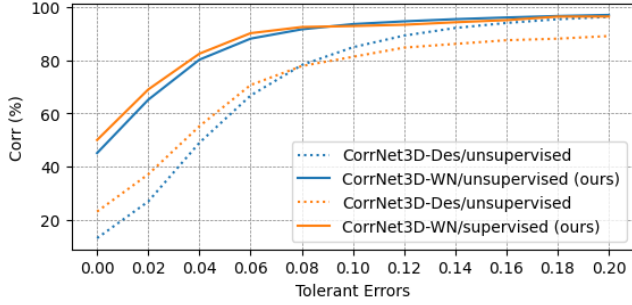
$$\text{Corr} = \frac{1}{N} \|\mathbf{P} \odot \mathbf{P}^{\text{gt}}\|_1, \quad (12)$$

$$\text{tolerant errors} = r / \text{dist}_{\max}, \quad (13)$$

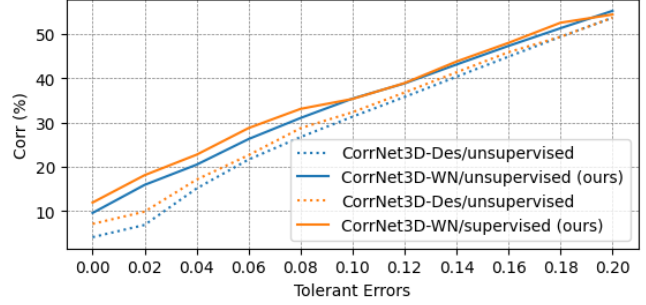
$$\text{dist}_{\max} := \max\{\|\mathbf{x}_i^A - \mathbf{x}_j^A\|, \forall i, j\}, \quad (14)$$

where \odot and $\|\cdot\|_1$ respectively represent the Hadamard product and L1-norm, and \mathbf{P}^{gt} and r respectively represent ground-truth correspondence matrix and tolerant radius.

Implementation details. In this experiment, we replaced the **DeSmooth module (DeS)** in the CorrNet3D model with our WN-based matching module (WN), which



(a) Test on the rigid dataset (surreal)



(b) Test on the non-rigid dataset (SHREC)

Figure 7. Accuracy transition of CorrNet3D w/ and w/o our matching module along with the tolerant errors defined in Eq. (13).

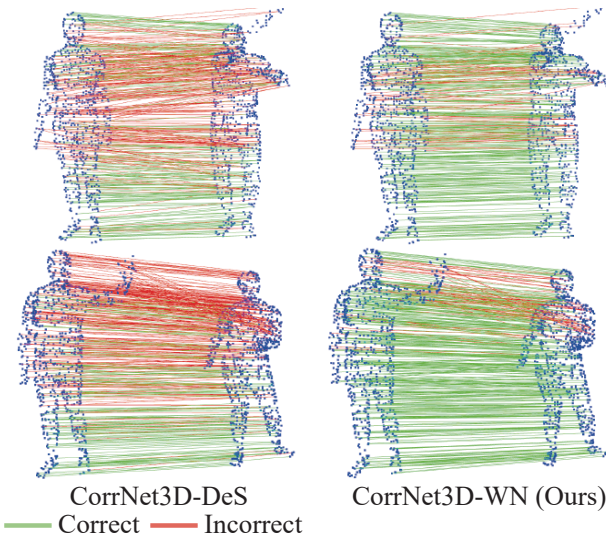


Figure 8. Visualization of improvement by the WN-based module on human shape data. Samples are randomly selected to avoid cherry-picking. Green lines show the exact match (i.e., tolerant error is zero).

was optimized according to the loss function in [47]. We set $r = 0.5$, $\mathcal{D}_s = 16$, and $L = 10$ for the parameters in the equations. Also, following [47], we trained the model with the Adam optimizer, a learning rate of $1e-4$, a batch size of 10, and 100 epochs.

Results on the rigid condition. The experimental results on the rigid dataset are shown in Fig. 7 (a). The result labeled CorrNet3D-WN shows the Corr metric score (\uparrow) of CorrNet3D with our WN-based matching module in the supervised/unsupervised settings, respectively. The figures shows the CorrNet3D-WN outperforms the CorrNet3D-DeS in both supervised and unsupervised settings, which further supported the versatility of our method.

A closer look at the figure shows that the performance

gain is significant for small tolerant error regions. It reveals that our method discriminatively finds the corresponding point from similar points.

Results on the non-rigid condition. Fig. 7 (b) shows the experimental results on the non-rigid dataset, and Fig. 8 shows the samples of the experimental results. Again, the CorrNet3D-WN outperforms the CorrNet3D-DeS in both the supervised and unsupervised settings. Note that their accuracies are lower than the rigid cases since they are trained with a rigid dataset following the original CorrNet3D experiment. Even under such a situation, our method boosted the performance.

5. Conclusion

This paper proposed a learning-based matching algorithm, Edge-Selective WeaveNet (ESWN), for 3D point cloud registration. The module was developed to shift a paradigm from only optimizing a feature extractor into optimizing both the feature extractor and a matching algorithm jointly, aiming to reach the global optimal solution. Our technical challenge was to scale the WeaveNet, an edge-wise feature forwarding architecture, by reducing its memory usage. We overcame this with radius-neighbor-based edge selection and feature splitting to compress initial edge-wise input to ESWN.

The experimental results demonstrated the consistent positive impact of our method on six datasets with four different SOTA architectures. A systematic analysis with a noise-controlled setting revealed the robustness of the matching module against uncertainty on extracted features. A memory consumption analysis revealed a limitation of our method, which still doubles the memory consumption.

Acknowledgments

This work was supported by JST-Mirai Program Grant Number JPMJMI21G2 and JSPS Kakenhi Grant Number 21K14130, Japan.

3D Point Cloud Registration with Learning-based Matching Algorithm

Supplementary Material

Method	ES	FS	train	eval.	NFMR(\uparrow)	IR(\uparrow)
WN			148.2 GiB	68.7 GiB	91.3	85.4
	✓		137.4 GiB	68.5 GiB	90.3	85.5
	✓		16.5 GiB	8.8 GiB	89.5	86.4
	✓	✓	10.3 GiB	5.8 GiB	88.7	87.9
DS	-	-	4.9 GiB	2.5 GiB	85.4	84.5

Table 5. Memory consumption test on 4DMatch with LNDP. ES and FS stand for Edge Selection and Feature Splitting, respectively.

Method	ES	FS	train	eval.	NFMR(\uparrow)	IR(\uparrow)
WN			151.5 GiB	80.5 GiB	91.2	83.2
	✓		143.2 GiB	72.1 GiB	90.1	84.2
	✓		18.7 GiB	10.4 GiB	89.5	85.4
	✓	✓	13.4 GiB	7.6 GiB	86.7	86.1
DS	-	-	6.5 GiB	3.5 GiB	83.7	82.7

Table 6. Memory consumption test on 4DMatch with Leopard. ES and FS stand for Edge Selection and Feature Splitting, respectively.

A. Additional Reports on Memory Consumption

Our method aims to improve memory efficiency to scale the original WeaveNet [30] for point cloud registration. An analysis of memory consumption, measured in actual training and inference on 4DMatch with RoITr, is shown in Subsec.4.2 and Table 3 of the main paper. We additionally show memory consumption results on 4DMatch in Tab. 5, Tab. 6 and 3DMatch in Tab. 7, Tab. 8, Tab. 9, which shows the same tendency as the result reported in the main paper.

The edge selection significantly decreases the memory consumption, while the performance is increased in IR (resp. IR, RR) and worse in NFMR (resp. FMR) in 4DMatch (resp. 3DMatch) dataset. Feature splitting at the connection between the feature extractor and the matching module further reduces memory consumption, with comparative NFMR (resp. FMR) and improved IR (resp. IR, RR) in 4DMatch (resp. 3DMatch) dataset. Overall, the analysis proved that our modification on WeaveNet is effective in both memory efficiency and accuracy.

Method	ES	FS	train	eval.	FMR(\uparrow)	IR(\uparrow)	RR(\uparrow)
WN			143.2 GiB	69.4 GiB	99.1	83.2	93.4
	✓		132.1 GiB	61.4 GiB	98.9	83.8	94.9
	✓		17.6 GiB	8.9 GiB	98.9	84.8	95.5
	✓	✓	9.9 GiB	5.4 GiB	98.9	86.8	96.2
OT	-	-	5.8 GiB	2.1 GiB	98.5	80.3	91.0

Table 7. Memory consumption test on 3DMatch with RoITr. ES and FS stand for Edge Selection and Feature Splitting, respectively.

Method	ES	FS	train	eval.	FMR(\uparrow)	IR(\uparrow)	RR(\uparrow)
WN			164.3 GiB	75.6 GiB	99.0	59.9	93.0
	✓		145.3 GiB	76.5 GiB	98.9	62.1	93.1
	✓		19.3 GiB	9.4 GiB	98.9	63.5	93.4
	✓	✓	10.3 GiB	6.4 GiB	98.6	65.6	94.1
DS	-	-	6.7 GiB	3.4 GiB	98.1	56.5	92.4

Table 8. Memory consumption test on 3DMatch with LNDP. ES and FS stand for Edge Selection and Feature Splitting, respectively.

Method	ES	FS	train	eval.	FMR(\uparrow)	IR(\uparrow)	RR(\uparrow)
WN			169.5 GiB	90.0 GiB	99.0	58.1	94.0
	✓		154.3 GiB	84.3 GiB	98.5	59.9	94.1
	✓		23.2 GiB	12.3 GiB	98.6	60.3	94.1
	✓	✓	12.7 GiB	6.9 GiB	98.4	64.5	95.7
DS	-	-	7.0 GiB	4.5 GiB	98.3	55.5	93.5

Table 9. Memory consumption test on 3DMatch with Leopard. ES and FS stand for Edge Selection and Feature Splitting, respectively.

Method	4DLoMatch		3DLoMatch		
	NFMR(\uparrow)	IR(\uparrow)	FMR(\uparrow)	IR(\uparrow)	RR(\uparrow)
DS	67.6	57.6	83.1	27.4	71.1
$r = 0.1$	70.3	58.9	87.1	27.9	73.1
WN $r = 0.5$	73.4	62.8	91.3	33.3	76.2
$r = 1.0$	71.1	60.0	88.3	30.6	72.7
$L = 6$	69.3	60.1	87.6	29.0	74.3
WN $L = 8$	71.3	62.2	90.1	32.3	75.8
$L = 10$	73.4	62.8	91.3	33.3	76.2
$\mathcal{D}_s = 4$	69.1	58.9	84.9	31.9	72.8
WN $\mathcal{D}_s = 16$	73.4	62.8	91.3	33.3	76.2
$\mathcal{D}_s = 64$	70.9	60.9	89.2	32.1	74.7

Table 10. Study on the impact of hyperparameters with LNDP. We set uncontrolled hyperparameters to our defaults (e.g., when r is varied, we used $L = 10$ and $\mathcal{D}_s = 16$).

Method	4DLoMatch		3DLoMatch		
	NFMR(\uparrow)	IR(\uparrow)	FMR(\uparrow)	IR(\uparrow)	RR(\uparrow)
DS	66.9	55.7	84.5	26.0	69.0
$r = 0.1$	68.2	54.1	80.4	25.6	63.5
WN $r = 0.5$	75.3	72.4	89.6	30.4	74.9
$r = 1.0$	69.3	58.9	88.6	30.6	74.0
$L = 6$	67.7	57.1	86.2	25.7	70.2
WN $L = 8$	68.7	57.2	87.2	27.8	73.5
$L = 10$	72.4	62.5	89.6	30.4	74.9
$\mathcal{D}_s = 4$	69.8	58.4	84.8	26.6	70.9
WN $\mathcal{D}_s = 16$	72.4	62.5	89.6	30.4	74.9
$\mathcal{D}_s = 64$	70.1	57.6	87.1	30.2	72.1

Table 11. Study on the impact of hyperparameters with Leopard. We set uncontrolled hyperparameters to our defaults (e.g., when r is varied, we used $L = 10$ and $\mathcal{D}_s = 16$).

B. Additional Reports on Hyperparameter Validation

Hyperparameter sensitivity against a dataset and combined feature extractors is an important factor of our method’s utility. Ablation studies on hyperparameter validation are shown in Subsec.4.4 and Table 4 of the main paper. We additionally show hyperparameter validation results on LNDP and Leopard in Tab. 10 and Tab. 11, which supports the validity of the setting under versatile situations.

Our method has three hyperparameters, r , L , and \mathcal{D}_s . We used the values directed in Subsec.4.1 as the defaults. Experimental results show that the default values always out-

performed the others regardless of the dataset. The detailed discussion is described in the main paper.

C. Network architecture

Our network architecture is the extended version of the conventional WeaveNet [30], and basic architecture follows its original network. This subsection additionally describes the original network architecture for reproducibility.

Network width The original network also contains the trainable linear layer $\phi_l^1(\cdot)$ and $\phi_l^2(\cdot)$ (appeared in Subsec.3.4 in the main paper). The input and output for each network are generally 16-dimensional features, and those dimensional settings achieve the best performance in various settings. Our network follows these dimensional settings since we also achieve the best performance in our task.

Input for WeaveNet Our network split the extracted features \mathbf{f}_n^A into $\mathbf{f}_n^{A_{\text{dis}}}$ and $\mathbf{f}_n^{A_{\text{point}}}$ (similarly, \mathbf{f}_m^B into $\mathbf{f}_m^{B_{\text{dis}}}$ and $\mathbf{f}_m^{B_{\text{point}}}$) and concatenate them for reducing the memory consumption as follows:

$$g(\mathbf{f}_n^{A_{\text{point}}}, \mathbf{f}_m^{B_{\text{point}}}) = \text{cat}(\mathbf{f}_n^{A_{\text{point}}}, d(\mathbf{f}_n^{A_{\text{dis}}}, \mathbf{f}_m^{B_{\text{dis}}}), \mathbf{f}_m^{B_{\text{point}}}), \quad (15)$$

where $d(\mathbf{f}_n^{A_{\text{dis}}}, \mathbf{f}_m^{B_{\text{dis}}})$ represents distance. The original WeaveNet does not split the extracted features and concatenates the extracted features since they only approximate NP-hard problems with lightweight edge-wise features. $g(\mathbf{f}_n^A, \mathbf{f}_m^B)$ in the original WeaveNet is defined as

$$g(\mathbf{f}_n^A, \mathbf{f}_m^B) = \text{cat}(\mathbf{f}_n^A, d(\mathbf{f}_n^A, \mathbf{f}_m^B), \mathbf{f}_m^B). \quad (16)$$

Experimental results in Tab.3 of the main paper (Tab. 5, Tab. 6, Tab. 7, Tab. 8, and Tab. 9 in this supplementary material) shows that the feature splitting contributes to reducing memory consumption and matching performance improvement.

References

- [1] Yasuhiro Aoki, Hunter Goforth, Rangaprasad Arun Srivatsan, and Simon Lucey. PointNetLK: Robust & efficient point cloud registration using pointnet. In *IEEE/CVF Conference on Computer Vision and Pattern Recognition*, pages 7163–7172, 2019. 2
- [2] Tiago Cortinhal, George Tzelepis, and Eren Erdal Aksoy. SalsaNext: Fast, uncertainty-aware semantic segmentation of LiDAR point clouds for autonomous driving. In *International Symposium on Advances in Visual Computing*, pages 207–222. Springer, 2020. 1
- [3] Marco Cuturi. Sinkhorn distances: Lightspeed computation of optimal transport. In *Advances in Neural Information Processing Systems*, 2013. 2
- [4] Nicolas Donati, Abhishek Sharma, and Maks Ovsjanikov. Deep geometric functional maps: Robust feature learning for shape correspondence. In *IEEE/CVF Conference on Computer Vision and Pattern Recognition*, pages 8592–8601, 2020. 5
- [5] Guoguang Du, Kai Wang, Shiguo Lian, and Kaiyong Zhao. Vision-based robotic grasping from object localization, object pose estimation to grasp estimation for parallel grippers: a review. *Artificial Intelligence Review*, 54(3):1677–1734, 2021. 1
- [6] Gil Elbaz, Tamar Avraham, and Anath Fischer. 3D point cloud registration for localization using a deep neural network auto-encoder. In *IEEE/CVF Conference on Computer Vision and Pattern Recognition*, pages 4631–4640, 2017. 2
- [7] Danièle Gibbons, Cheng-Chew Lim, and Peng Shi. Deep learning for bipartite assignment problems. In *IEEE International Conference on Systems, Man and Cybernetics*, pages 2318–2325, 2019. 3
- [8] Thibault Groueix, Matthew Fisher, Vladimir G. Kim, Bryan Russell, and Mathieu Aubry. 3D-CODED: 3D correspondences by deep deformation. In *European Conference on Computer Vision*, pages 230–246, 2018. 5
- [9] Yulan Guo, Mohammed Bennamoun, Ferdous Sohel, Min Lu, Jianwei Wan, and Ngai Ming Kwok. A comprehensive performance evaluation of 3D local feature descriptors. *International Journal of Computer Vision*, 116(1):66–89, 2016. 2
- [10] Yulan Guo, Hanyun Wang, Qingyong Hu, Hao Liu, Li Liu, and Mohammed Bennamoun. Deep learning for 3D point clouds: A survey. *IEEE Transaction on Pattern Analysis and Machine Intelligence*, 2020. 2
- [11] Xian-Feng Hana, Jesse S Jin, Juan Xie, Ming-Jie Wang, and Wei Jiang. A comprehensive review of 3D point cloud descriptors. *arXiv preprint arXiv:1802.02297*, 2, 2018. 2
- [12] Binh-Son Hua, Minh-Khoi Tran, and Sai-Kit Yeung. Point-wise convolutional neural networks. In *IEEE/CVF Conference on Computer Vision and Pattern Recognition*, pages 984–993, 2018. 2
- [13] Shengyu Huang, Zan Gojcic, Mikhail Usvyatsov, Andreas Wieser, and Konrad Schindler. Predator: Registration of 3D point clouds with low overlap. In *IEEE/CVF Conference on Computer Vision and Pattern Recognition*, pages 4267–4276, 2021. 2, 5
- [14] Andrew E Johnson and Martial Hebert. Using spin images for efficient object recognition in cluttered 3D scenes. *IEEE Transaction on Pattern Analysis and Machine Intelligence*, 21(5):433–449, 1999. 2
- [15] Harold W. Kuhn. The hungarian method for the assignment problem. *Naval Research Logistics Quarterly*, 2:83–97, 1955. 2
- [16] Bo Li, Yijuan Lu, Chunyuan Li, Afzal Godil, Tobias Schreck, Masaki Aono, Martin Burtcher, Qiang Chen, Nihad Karim Chowdhury, Bin Fang, et al. A comparison of 3D shape retrieval methods based on a large-scale benchmark supporting multimodal queries. *Computer Vision and Image Understanding*, 131:1–27, 2015. 7
- [17] Qimai Li, Zhichao Han, and Xiao-Ming Wu. Deeper insights into graph convolutional networks for semi-supervised learning. In *AAAI Conference on Artificial Intelligence*, pages 3538–3545, 2018. 3
- [18] Yang Li and Tatsuya Harada. Leopard: Learning partial point cloud matching in rigid and deformable scenes. In *IEEE/CVF Conference on Computer Vision and Pattern Recognition*, pages 5554–5564, 2022. 2, 5
- [19] Yang Li and Tatsuya Harada. Non-rigid point cloud registration with neural deformation pyramid. *Advances in Neural Information Processing Systems*, 35:27757–27768, 2022. 2, 5
- [20] Weiping Liu, Jia Sun, Wanyi Li, Ting Hu, and Peng Wang. Deep learning on point clouds and its application: A survey. *Sensors*, 19(19):4188, 2019. 1
- [21] Xu Ma, Can Qin, Haoxuan You, Haoxi Ran, and Yun Fu. Rethinking network design and local geometry in point cloud: A simple residual MLP framework. In *International Conference on Learning Representation*, 2022. 2
- [22] Daniel Maturana and Sebastian Scherer. VoxNet: A 3D convolutional neural network for real-time object recognition. In *IEEE/RSJ International Conference on Intelligent Robots and Systems*, pages 922–928, 2015. 2
- [23] Kenta Oono and Taiji Suzuki. Graph neural networks exponentially lose expressive power for node classification. In *International Conference on Learning Representation*, 2020. 3
- [24] Charles R Qi, Hao Su, Kaichun Mo, and Leonidas J Guibas. PointNet: Deep learning on point sets for 3D classification and segmentation. In *IEEE/CVF Conference on Computer Vision and Pattern Recognition*, 2017. 2, 4
- [25] Charles R Qi, Li Yi, Hao Su, and Leonidas J Guibas. PointNet++: Deep hierarchical feature learning on point sets in a metric space. In *Advances in Neural Information Processing Systems*, 2017. 2
- [26] Ignacio Rocco, Mircea Cimpoi, Relja Arandjelović, Akihiko Torii, Tomas Pajdla, and Josef Sivic. Neighbourhood consensus networks. In *Advances in Neural Information Processing Systems*, 2018. 2
- [27] Paul-Edouard Sarlin, Daniel DeTone, Tomasz Malisiewicz, and Andrew Rabinovich. SuperGlue: Learning feature matching with graph neural networks. In *IEEE/CVF Conference on Computer Vision and Pattern Recognition*, 2020. 2

- [28] Vinit Sarode, Xueqian Li, Hunter Goforth, Yasuhiro Aoki, Rangaprasad Arun Srivatsan, Simon Lucey, and Howie Choset. PCRNet: Point cloud registration network using pointnet encoding. *arXiv preprint arXiv:1908.07906*, 2019. [2](#)
- [29] N Senin, S Catalucci, M Moretti, and RK Leach. Statistical point cloud model to investigate measurement uncertainty in coordinate metrology. *Precision Engineering*, 70: 44–62, 2021. [1](#)
- [30] Shusaku Sone, Jiaxin Ma, Atsushi Hashimoto, Naoya Chiba, and Yoshitaka Ushiku. Weavenet for approximating two-sided matching problems. *arXiv preprint arXiv:2310.12515*, 2023. [3](#), [6](#), [9](#), [10](#)
- [31] Jiaming Sun, Zehong Shen, Yuang Wang, Hujun Bao, and Xiaowei Zhou. LoFTR: Detector-free local feature matching with transformers. In *IEEE/CVF Conference on Computer Vision and Pattern Recognition*, pages 8922–8931, 2021. [2](#)
- [32] Yang-Tian Sun, Qian-Cheng Fu, Yue-Ren Jiang, Zitao Liu, Yu-Kun Lai, Hongbo Fu, and Lin Gao. Human motion transfer with 3D constraints and detail enhancement. *IEEE Transaction on Pattern Analysis and Machine Intelligence*, 45(4): 4682–4693, 2023. [1](#)
- [33] Federico Tombari, Samuele Salti, and Luigi Di Stefano. Unique signatures of histograms for local surface description. In *European Conference on Computer Vision*, pages 356–369. Springer, 2010. [2](#)
- [34] Gül Varol, Javier Romero, Xavier Martin, Naureen Mahmood, Michael J. Black, Ivan Laptev, and Cordelia Schmid. Learning from synthetic humans. In *Proceedings of the IEEE Conference on Computer Vision and Pattern Recognition*, 2017. [7](#)
- [35] Shenlong Wang, Simon Suo, Wei-Chiu Ma, Andrei Pokrovsky, and Raquel Urtasun. Deep parametric continuous convolutional neural networks. In *IEEE/CVF Conference on Computer Vision and Pattern Recognition*, pages 2589–2597, 2018. [2](#)
- [36] Yue Wang and Justin M Solomon. Deep closest point: Learning representations for point cloud registration. In *Proceedings of the IEEE/CVF International Conference on Computer Vision*, pages 3523–3532, 2019. [2](#)
- [37] Yue Wang, Yongbin Sun, Ziwei Liu, Sanjay E Sarma, Michael M Bronstein, and Justin M Solomon. Dynamic graph cnn for learning on point clouds. *ACM Transactions on Graphics*, 38(5):1–12, 2019. [2](#)
- [38] Saining Xie, Sainan Liu, Zeyu Chen, and Zhuowen Tu. Attentional shapecontextnet for point cloud recognition. In *IEEE/CVF Conference on Computer Vision and Pattern Recognition*, pages 4606–4615, 2018.
- [39] Yifan Xu, Tianqi Fan, Mingye Xu, Long Zeng, and Yu Qiao. SpiderCNN: Deep learning on point sets with parameterized convolutional filters. In *European Conference on Computer Vision*, pages 87–102, 2018. [2](#)
- [40] Jiaqi Yang, Qian Zhang, Ke Xian, Yang Xiao, and Zhiguo Cao. Rotational contour signatures for both real-valued and binary feature representations of 3D local shape. *Computer Vision and Image Understanding*, 160:133–147, 2017. [2](#)
- [41] Jiaqi Yang, Qian Zhang, Yang Xiao, and Zhiguo Cao. TOLDI: An effective and robust approach for 3D local shape description. *Pattern Recognition*, 65:175–187, 2017. [2](#)
- [42] Zi Jian Yew and Gim Hee Lee. RPM-Net: Robust point matching using learned features. In *IEEE/CVF Conference on Computer Vision and Pattern Recognition*, pages 11824–11833, 2020. [2](#)
- [43] Hao Yu, Fu Li, Mahdi Saleh, Benjamin Busam, and Slobodan Ilic. CoFiNet: Reliable coarse-to-fine correspondences for robust pointcloud registration. *Advances in Neural Information Processing Systems*, 34, 2021. [2](#)
- [44] Hao Yu, Zheng Qin, Ji Hou, Mahdi Saleh, Dongsheng Li, Benjamin Busam, and Slobodan Ilic. Rotation-invariant transformer for point cloud matching. In *IEEE/CVF Conference on Computer Vision and Pattern Recognition*, pages 5384–5393, 2023. [2](#), [5](#)
- [45] Manzil Zaheer, Satwik Kottur, Siamak Ravanbakhsh, Barnabas Poczos, Russ R Salakhutdinov, and Alexander J Smola. Deep sets. In *Advances in Neural Information Processing Systems*, 2017. [2](#), [4](#)
- [46] Andy Zeng, Shuran Song, Matthias Nießner, Matthew Fisher, Jianxiong Xiao, and Thomas Funkhouser. 3DMatch: Learning local geometric descriptors from rgb-d reconstructions. In *IEEE/CVF Conference on Computer Vision and Pattern Recognition*, pages 1802–1811, 2017. [2](#), [5](#)
- [47] Yiming Zeng, Yue Qian, Zhiyu Zhu, Junhui Hou, Hui Yuan, and Ying He. CorrNet3D: Unsupervised end-to-end learning of dense correspondence for 3D point clouds. In *IEEE/CVF Conference on Computer Vision and Pattern Recognition*, pages 6052–6061, 2021. [2](#), [5](#), [7](#), [8](#)
- [48] Zhiyuan Zhang, Binh-Son Hua, and Sai-Kit Yeung. Shellnet: Efficient point cloud convolutional neural networks using concentric shells statistics. In *International Conference on Computer Vision*, pages 1607–1616, 2019. [2](#)
- [49] Zhiyuan Zhang, Yuchao Dai, and Jiadai Sun. Deep learning based point cloud registration: an overview. *Virtual Reality & Intelligent Hardware*, 2(3):222–246, 2020. [2](#)
- [50] Yu Zheng, Xiuwei Xu, Jie Zhou, and Jiwen Lu. PointRas: Uncertainty-aware multi-resolution learning for point cloud segmentation. *IEEE Transactions on Image Processing*, 31: 6002–6016, 2022. [1](#)
- [51] Yu Zhong. Intrinsic shape signatures: A shape descriptor for 3D object recognition. In *International Conference on Computer Vision Workshop*, pages 689–696. IEEE, 2009. [2](#)